Mechanical loading potentiates the bone response of anabolic osteoporosis treatments through mechanoregulation at the tissue level

Authors: Friederike A. Schulte[1†], Julia K. Griesbach[1†], Claudia Weigt, Marcella von Salis-Soglio[1], Floor M. Lambers[1], Francisco C. Marques[1], Michaela Kneissel[3], Pete J. Richards[2,3], Gisela A. Kuhn[1], Ralph Müller[1*]

Affiliations:

[1]Institute for Biomechanics, ETH Zurich; Zurich, Switzerland.
[2]Bone and Stem Cell Research Group, CABMM, University of Zurich; Zurich, Switzerland.
[3]Musculoskeletal Disease Area, Novartis Institutes for Biomedical Research; Basel, Switzerland.

[*]Corresponding author. Email: ram@ethz.ch
[†]These authors contributed equally to this work.

One Sentence Summary:

Mechanoregulation at the tissue level induced by mechanical loading increases targeted remodeling in bisphosphonate, parathyroid hormone, or sclerostin antibody treatment.

Abstract: Bone loss in postmenopausal osteoporosis is caused by a remodeling imbalance towards increased bone resorption. Existing osteoporosis therapies are systemic and designed to recover bone mass, using the same molecular pathways that also allow bone to adapt to changing mechanical demands. Supraphysiological mechanical loading induces use a process on the tissue level called mechanoregulation, ensuring that bone is formed where needed and resorbed where unneeded. Little focus has been on combination therapy of physical and pharmaceutical therapy. Here, we report the effects of combining physical therapy in the form of mechanical loading with pharmaceutical treatment, i.e. bisphosphonates (BIS), parathyroid hormone (PTH), or sclerostin antibodies (SclAB) in ovariectomized C57Bl/6J mice. Mechanical loading synergistically potentiated trabecular bone mass under PTH or SclAB therapy but only marginally increased trabecular bone mass under BIS treatment. Bone remodeling was targeted to underlying micro-mechanical stimuli through mechanoregulation in all pharmaceutical treatments, but to different extents. BIS treatment showed higher untargeted remodeling compared to anabolic treatments, both alone and in combination with mechanical loading. Mechanical loading potentiated the mechanoregulatory response of SclAB treatment (synergistically) and PTH treatment (additively), indicating that in anabolic treatments, mechanical loading potentiates treatment efficacy by inducing more targeted bone formation and resorption. These findings suggest that incorporating physical therapy into anabolic pharmaceutical treatment regimens holds promise for enhancing therapeutic outcomes in osteoporosis management.

INTRODUCTION

Bone has been known for its ability to functionally adapt to the mechanical demands: overloaded bones increase their density and disused bones decrease their density, a concept referred to as mechanostat (*1, 2*). Trabecular bone demonstrates particular sensitivity to altering mechanical demands since individual trabeculae have the freedom to remodel towards an optimal load distribution. Global mechanical demands are translated to the tissue level where osteoblasts form bone and osteoclasts resorb bone, a process called bone (re)modeling. Load transfer to the local mechanical environment enables osteocytes to stimulate osteoclast activity in low-strain areas and osteoblast activity in high-strain areas. This concept of mechanoregulation has been supported by combined *in vivo* experiments and micro-finite element simulations in mice (*3, 4*) and humans (*5, 6*) in trabecular bone at the tissue level. Also, small portions of site-unspecific non-targeted bone (re)modeling occur, related to maintaining mineral homeostasis (*7, 8*).

Osteoporosis is a bone disease affecting approximately 500 million people worldwide (*9*) and characterized by an imbalance in (re)modeling towards resorption, which leads to deterioration of bone mass, decreased bone strength, and increased risk of fractures. Pharmaceutical treatments use cellular and molecular pathways that allow bone to adapt to changing mechanical demands. Anti-catabolic treatments, particularly bisphosphonates, decrease resorption rates by poisoning the osteoclasts and are the mainstay of current therapeutic interventions. While bisphosphonates are mostly well tolerated (*10*), adverse side effects such as jaw necrosis have led to reduced compliance rates and increased interest into alternatives. Parathyroid hormone (PTH) is a hormone responsible for calcium release. Intermittently applied, it acts as an anabolic treatment and leads to a net increase in bone mass and strength. Sclerostin antibody therapy, a recently emerging anabolic treatment, inhibits sclerostin, an antagonist of the Wnt-signaling pathway (*11*). The activated Wnt-signaling pathway, i.e. the effect of sclerostin antibody therapy, stimulates osteoblastic bone formation and inhibits osteoclastic bone resorption. Sclerostin antibody therapy has an anabolic window of 12 months until saturation, after which time other therapies need to be explored.

Besides pharmaceutical treatments, physical exercise has been reported to have positive effects on the risk reduction of major osteoporotic fractures (*12*). Supraphysiological mechanical loading increases bone mass, decreases bone loss, and improves bone strength (*13*). Additionally, *in vivo* studies have shown the potential to increase the sensitivity of the bone's mechanoregulation mechanisms, thereby ensuring induced bone gain is more targeted to the mechanical need of the bone (*14, 15*). Therefore, mechanical loading might have the capacity to improve the efficacy of pharmaceutical treatments in fracture risk reduction. Both therapies could be easily combined.

Previously, using preclinical animal models, mechanical loading did not interfere with bisphosphonate treatment, neither in trabecular nor in cortical regions of tibias in C57Bl/6 mice (*16*). Intermittent administration of PTH at 20-80 μg/kg/day interacted synergistically with artificially applied mechanical loading to increase bone mass in young healthy mice (*17*). In 19-month-old healthy mice, it led to additive benefits in the periosteal cortical regions of the tibia (*18*). Mechanical loading combined with sclerostin antibodies in young healthy mice led to a synergistic increase in cortical bone mass (*19*). Robinson et al. reported synergistic effects in the trabecular compartment of the healthy tibia, but only prevalent in regions that were not remodeling- but only modeling-based (*20*).

While effects of pharmaceutical treatments and their combination with mechanical loading on bone morphometry have been investigated, their effects on mechanoregulation in trabecular bone remain unclear. Assessing if increased bone mass recovery resulting from pharmaceutical treatments is targeted to mechanical demands would help understand their efficacy in fracture prevention. The aims of the current study were to investigate to which extent I) mechanical loading combined with pharmaceutical treatment improves trabecular bone mass, architecture, and strength, I) pharmaceutical treatments target sites in need of adaptation at the tissue level, and III) pharmaceutical treatments alter the sensibility of mechanoregulation mechanisms.

To address these aims we used a highly controlled bone loading model, that has in the past led to 20% increases in trabecular bone mass in healthy animals (*21*). We administered bisphosphonate, PTH, or sclerostin antibody treatment to ovariectomized 20-week-old C57Bl/6J mice. Time-lapsed micro-computed tomography derived bone formation and resorption clusters were compared with their finite-element-derived micro-mechanical environment. We found synergistic effects in trabecular bone volume fraction for mechanical loading for anabolic treatments PTH and sclerostin antibodies. Using conditional probability and remodeling velocity analyses, we identified local differences in the sensibility of mechanoregulation mechanisms, which may explain the synergisms in the trabecular bone response to anabolic pharmaceutical therapies combined with mechanical loading. Our results suggest increased adaptation to mechanical demands under anabolic treatments potentiates the effects on fracture risk reduction. These findings are relevant when considering physical therapy as an adjunct to pharmaceutical treatment of postmenopausal osteoporosis.

RESULTS

Monotreatments increase trabecular bone mass via different remodeling effects

C57Bl/6J mice were ovariectomized at 15 weeks-of-age. All animals lost bone mass in response to ovariectomy as verified by *in vivo* time-lapsed micro-computed tomography of the trabecular region of the 6th caudal vertebra (in total -21.7±11.6% change in trabecular bone volume fraction compared to start of treatment, ΔBV/TV). From week 20 to 24, animals received pharmaceutical treatment and/or mechanical loading (Fig. 1A). The vehicle-group (VEH)

resulted in a further decrease in BV/TV between weeks 20 and 24 (-10.8%, Fig. 1B). In all monotreatment groups, BV/TV increased significantly over four weeks (Fig. 1B; mechanical loading (ML): 14.3%; bisphosphonate treatment group (BIS): 13.5%; parathyroid hormone treatment group (PTH): 17.5%; sclerostin antibody treatment group (SclAB): 21.5%).

The BIS group showed no significant increase in trabecular thickness (Tb.Th: +4.2%) compared to the VEH group (+0.5%), while the anabolic treatment groups including the ML group increased Tb.Th (ML: +19.4%, PTH: +10.6%, SclAB: +24.1%), with the PTH group significantly less pronounced than the other anabolic treatment groups (Fig. 1C). Trabecular number (Tb.N; Fig. 1 D) went down in the VEH group (VEH: -8.2%), was preserved in the BIS group (+2.7%), and went down in all other groups (ML: -8.5%; PTH: -7.0%; SclAB:-10.3%). Since in the PTH group, the net increase in BV/TV could not be explained with increased Tb.Th or preserved Tb.N, the cortex was taken into account. While cortical BV/TV increased in all treatment groups (VEH: -1.4%, ML: +6.4%, BIS: +3.4%, PTH: +8.1%, SclAB: +14.4%), the cortical surface per tissue volume (Ct.BS/TV) was only increased in the PTH group (+13.0%), indicating a potential trabecularization of the inner parts of the cortex (Fig. 1E).

Bone formation and resorption rates were calculated from registration and binarization of consecutive micro-CT scans (Fig. 1F). As shown in Fig. 1G-L, the BIS group showed unchanged bone formation parameters from the VEH group with being significantly lower than the PTH and the SclAB group (bone formation rate per bone volume (BFR/BV): VEH: 1.3%/d, ML: 1.4%/d, BIS: 1.0%/d, PTH: 1.5%/d, SclAB: 1.6%/d, Fig. 1G). Mineral apposition rate (MAR) was not affected in any monotreatment group (Fig. 1H). The anabolic ML, PTH, and SclAB groups increased mineralizing surface (MS) significantly compared to VEH or BIS (VEH: 41.2%, ML: 56.5%, BIS: 42.4%, PTH: 63.3%, SclAB: 68.0%, Fig. 1I).

Bone resorption rate (BRR) was significantly reduced in all monotreatments including ML compared to the VEH group (VEH: 1.4%/d; BIS: 0.6%/d; ML: 0.7%/d; PTH: 0.5%/d; SclAB: 0.5%/d; Fig. 1J). Mineral resorption rate (MRR) was significantly reduced in the BIS group compared to the VEH group, being unchanged in the anabolic treatment groups (Fig. 1K). In the anabolic treatment groups, eroded surface (ES) was significantly reduced compared to the VEH or the BIS group (VEH: 30.6%; BIS: 29.5%; ML: 22.0%; PTH: 19.5%; SclAB: 14.0%; Fig. 1L).

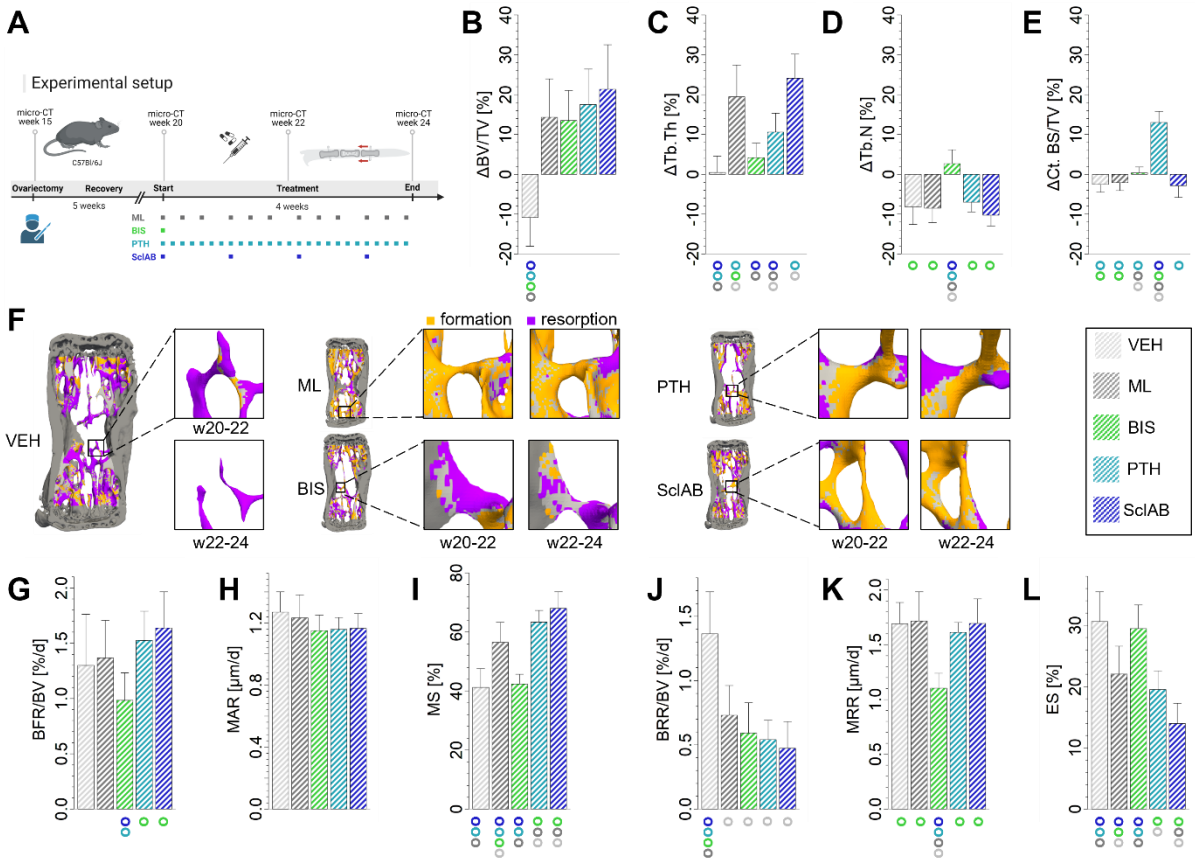

Figure 1: Monotreatments increase trabecular bone mass in ovariectomized animals by different remodeling mechanisms. *(**A**) Experimental setup. 15-week-old mice are ovariectomized and treatment is administered between week 20 (w20) and 24 (w24) with biweekly micro-computed tomography scans. Created with Biorender (**B-E**) Mono-treatments (VEH: n=29, BIS: n=9, PTH: n=10, SclAB: n=9), barplots show percentage change from treatment start at w20 over four weeks in (**B**) bone volume fraction ΔBV/TV, (**C**) trabecular thickness ΔTb.Th, (**D**) trabecular number ΔTb.N (**E**) cortical bone surface per tissue volume ΔCt. BS/TV (**F**) representative micro-computed tomography overlays at weeks 20-22 and 22-24 from monotreatment groups, with formation and resorption volumes generated from rigid image registration (**G-L**) Dynamic morphometric rates calculated from time interval w22-w24 (**G**) bone formation rate per bone volume BFR/BV (**H**) mineral apposition rate MAR (**I**) mineralizing surface MS (**J**) bone resorption rate per bone volume BRR/BV (**K**) mineral resorption rate MRR (**L**) eroded surface ES. p<0.05 compared to the treatment group in the respective color: o: monotreatment ● combination treatment.*

Increases in trabecular bone volume fraction are synergistic for SclAB and PTH

To investigate the extent to which mechanical loading could further increase the pharmaceutical bone response, we applied supraphysiological mechanical loading to the 6th caudal vertebra through a mechanical loading device using stainless steel pins in the adjacent vertebrae. Representative inlets of the adapting structures over the two measured time intervals are shown in Fig. 2A-C. The combination treatment BIS + ML resulted in 25.5% increase in ΔBV/TV, as compared to 13.5% in BIS or 14.3% in ML (Fig. 2D, Table 1). The response for combined treatment BIS + ML was higher than for both monotreatments but did not exceed the sum of the single treatment responses (Fig. 2E). The combination treatment PTH + ML showed a ΔBV/TV of 40.1% which was significantly higher compared to the bone responses of monotreatment PTH of 17.5% (Fig. 2E), indicating a synergistic effect in ΔBV/TV. The SclAB + ML group showed an increase in BV/TV of 49.5% where the SclAB + ML group exceeded the sum of monotreatment responses (SclAB: +21.5%, Fig. 2E), thus indicating a synergistic effect in ΔBV/TV. ΔTb.Th in the BIS + ML group was significantly higher than in the BIS group (Fig. 2F), to an extent comparable to the ML-group. Tb.Th was significantly higher than in the PTH-group after four weeks, but the effect for Tb.Th could only be considered additive

(Fig. 2G). The SclAB + ML group exceeded the sum of monotreatment responses of ΔTb.Th (Fig. 2G).

In the BIS + ML group, ΔTb.N was preserved even with additional mechanical loading (Fig. 2H). Interestingly, ML as a monotreatment had reduced Tb.N, and this effect was blunted by additional BIS treatment, as can be seen in Fig. 2H. The loss of Tb.N observed in SclAB could not be reverted in SclAB + ML. SclAB + ML exceeded the sum of monotreatment responses of cortical BV/TV and cortical thickness (ΔCt.Th; Fig. 2J-M). Ct. BS/TV, indicating trabecularization of the cortical shell, was highest in the PTH and PTH + ML groups (Fig. 2N). Compared to the PTH group, trabecularization of the cortical shell was partially blunted by combined mechanical loading, as can be seen in the PTH + ML group (Fig. 2N,O).

BFR was significantly increased in PTH + ML and SclAB + ML compared to their monotreatments (Fig. 2P,Q), primarily through increases in MS (Fig. 2T,U). At the same time, BRR was significantly reduced in all combination groups (Fig. 2V,W), through decreases in both MRR and ES (Fig. 2X-AA). The observed reduced MRR by BIS treatment was not altered by mechanical loading (Fig. 2X,Y). The synergistic bone response of SclAB + ML resulted from synergistically increased BFR and MAR (Fig. 2Q,S), and additive effects in MS (Fig. 2U). On the resorption side, synergistic decreases in ES (Fig. 2AA) and additive decreases in BRR and MRR (Fig. 2W,Y).

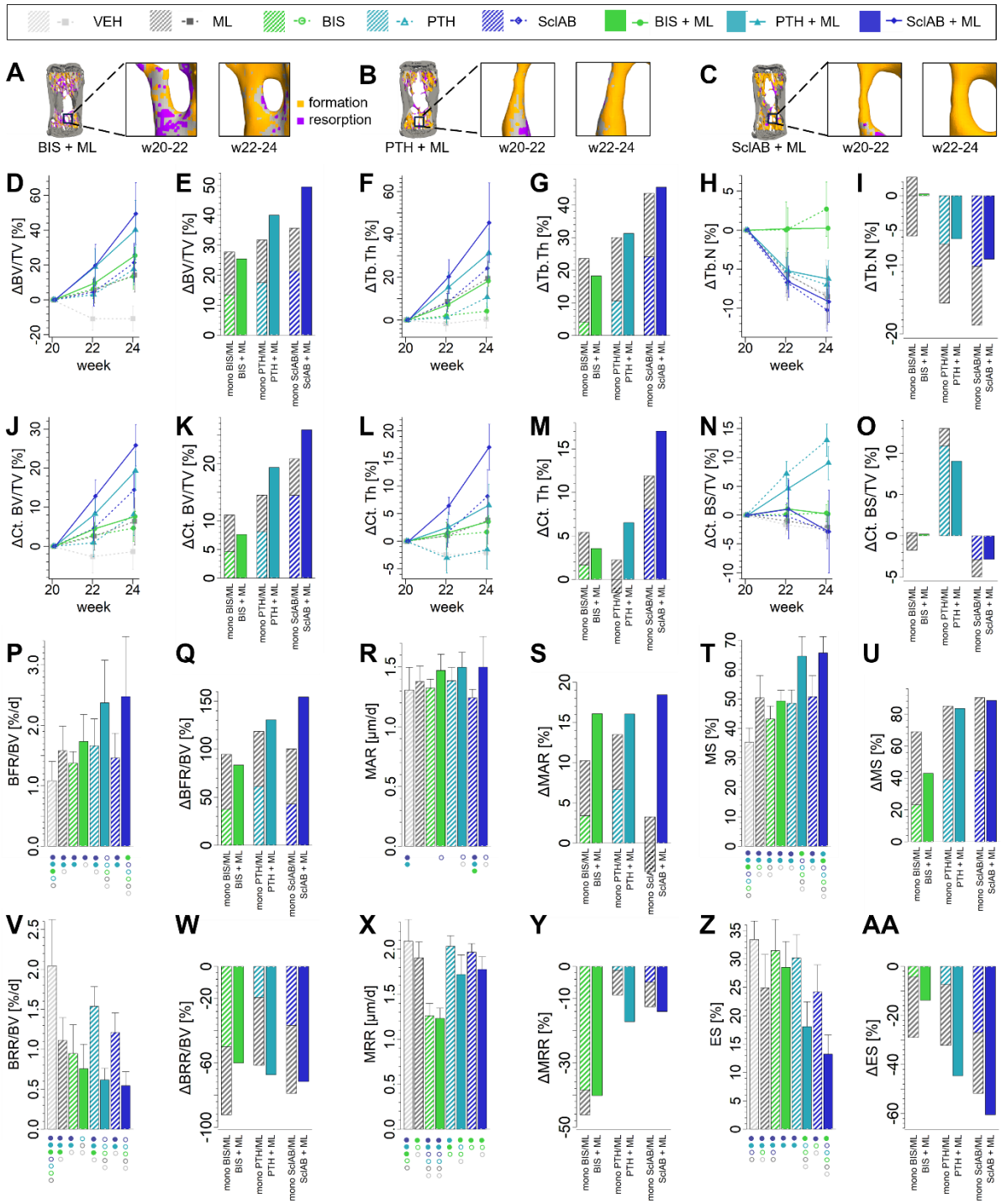

Figure 2: Loading potentiates the morphometric effects of anabolic pharmaceutical treatments. *(**A-C**) Visual representations of combination groups BIS + ML, PTH + ML, and SclAB + ML in time intervals week (w) 20-22 and 22-24 (**D**) Change in bone volume fraction compared to week 20 (ΔBV/TV) (**E**) Responses in ΔBV/TV of monotreatment groups compared to combined treatment response (**F**) Change in trabecular thickness (ΔTb.Th) (**G**) ΔTb.Th as sum of single treatment responses compared to combined treatment response (**H**) Change in trabecular number (ΔTb.N). (**I**) Sum of single treatment responses in Tb.N compared to combined treatment response (J) Change in cortical BV/TV (ΔCt. BV/TV) (**K**) Sum of single treatment responses in Ct.BV/TV compared to combined treatment response (**L**) Change in cortical thickness (ΔCt.Th) (**M**) Sum of single treatment responses in Ct.Th compared to combined treatment response (**N**) Cortical BS/TV normalized to week 20 (ΔCt. BS/TV) (**O**) Sum of single treatment responses in Ct.BS/TV compared to combined treatment response (**P-U**) Dynamic bone morphometry calculated from registration of time-lapsed in vivo micro-computed tomography at biweekly time intervals week 20-22. (**P**) bone formation rate per bone volume (BFR/BV) (**Q**) sum of ΔBFR/BV of monotreatments compared to combination treatment (**R**) mineral apposition rate (MAR) (**S**) sum of ΔMAR of monotreatments compared to combination treatment (**T**) mineralizing surface (MS) (**U**) sum of ΔMS of monotreatments compared to combination treatment*

*(**V**) bone resorption rate per bone volume (BRR/BV) (**Y**) sum of ΔBRR/BV of monotreatments compared to combination treatment (**X**) mineral resorption rate (MRR) (**Y**) sum of ΔMRR of monotreatments compared to combination treatment (**Z**) eroded surface (ES); (**AA**) sum of ΔES of monotreatments compared to combination treatment p<0.05 compared to the treatment group in the respective color: o: monotreatment ●: combination treatment.*

Table 1: Significance levels of static morphometric parameters as difference from end of treatment at week 24 to start of treatment at week 20. *p<0.05 as compared to the respective treatment group o: monotreatment; ● combination treatment*

Parameter	VEH	ML	BIS	BIS + ML	PTH	PTH + ML	SclAB	SclAB + ML
ΔBV/TV [%]	oooo ●●●	o ●●●	o ●●	oo ●●	o ●●	oooo ●●	o ●●	oooo ●
ΔTb.Th [%]	ooo ●●●	ooo ●●	ooo ●●●	oooo ●●	ooo ●●●	oooo ●●	ooo ●●	oooo ●●
ΔTb.N [%]	o ●	o ●	oooo ●●	ooo ●●	o ●	o ●	o ●	o ●
ΔCt.BV/TV [%]	oooo ●●●	o ●●	oo ●●	o ●●	oo ●●	oooo ●●	oooo ●●	oooo ●●
ΔCt.Tb.Th [%]	ooo ●●●	oo ●	ooo ●●	oo ●	ooo ●●●	ooo ●	ooo ●	oooo ●●
ΔCt.BS/TV [%]	oo ●●	o ●●	oo ●	ooo ●	oooo ●●●	oooo ●●	o ●	o ●

Increases in strength are additive for PTH and synergistic for SclAB treatment

Decreased strength has been correlated to increased fracture risk. To investigate if increases in BV/TV were associated with increased trabecular strength, we performed micro-finite element analysis and assessed mechanical properties of resulting structures after 4 weeks of pharmaceutical and/or mechanical treatment. Mean and maximum strain energy density (SED) and (SED_{max}) in the trabecular compartment decreased over the course of 4 weeks in all treatments but not in the VEH group, being most pronounced in the combination groups (Fig. 3B,D, Table 2). The decreases in mean SED in the trabecular compartment in all combination groups were less than additive (Fig. 3C,E). SED and SED_{max} correlated strongly over all groups (R^2=0.97, Fig. 3F). Trabecular strength increased in all groups but not in the VEH group, with SclAB + ML demonstrating the highest increase (Fig. 3G, Table 2). Trabecular strength increased additively in the PTH + ML group and synergistically in the SclAB + ML group (Fig. 3H). The BIS + ML group benefitted from trabecular strength increases, but not as pronounced as with both single treatments. The initial trabecular strength of a vertebra correlated moderately with BV/TV (R^2=0.4, Fig. 3I), after 2 weeks of treatment with R^2=0.64 (Fig. 3J), and after 4 weeks with R^2=0.84, indicating the increases in bone mass over time lead to an increased strength of the trabecular bone.

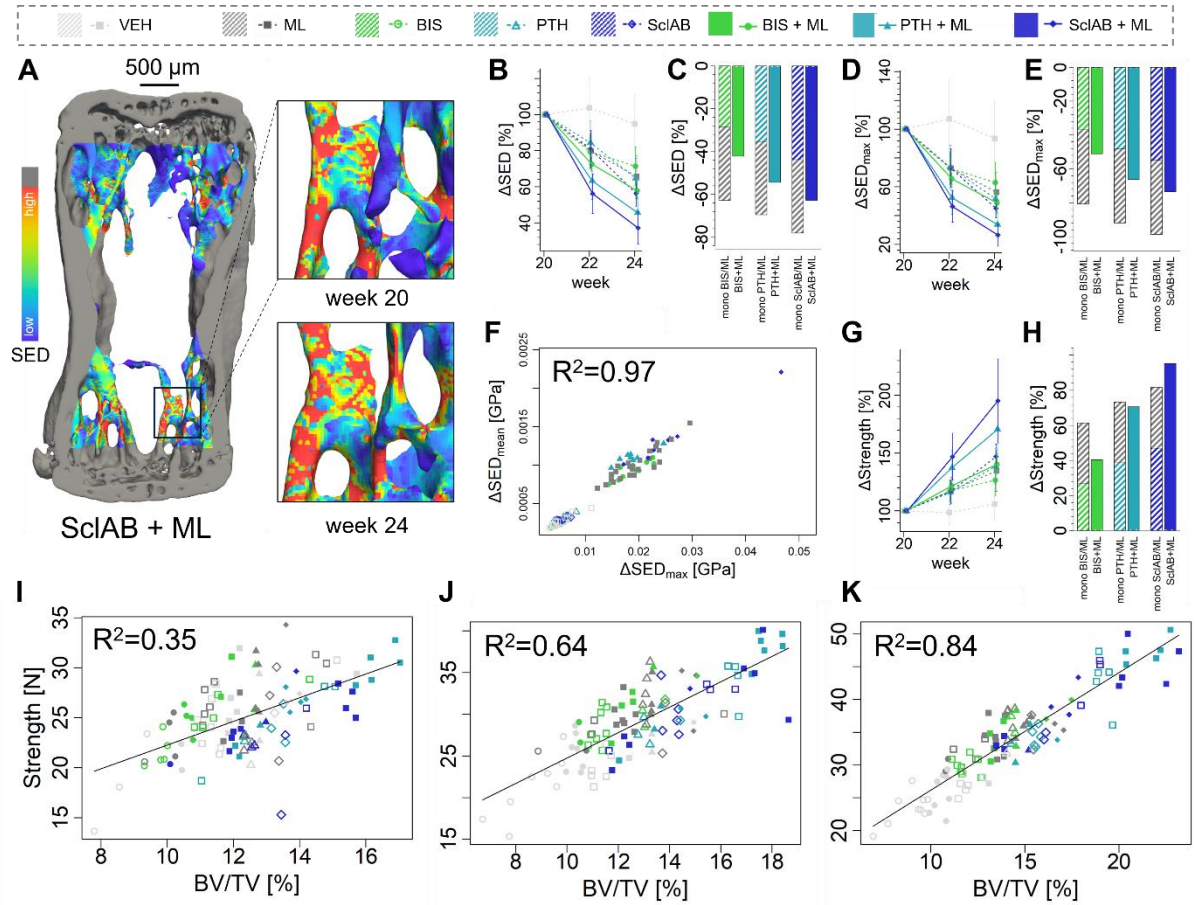

Figure 3: Strength increases in all treatment groups. *(**A**) Representative image of finite element model where the colored structures indicate the level of strain energy density in the analyzed region of trabecular bone and a zoom-in on a trabecular detail at week 20 and at week 24, showing an increase in trabecular thickness at a site of high preceding strain energy density and resulting reduction of high strain. (**B**) Mean strain energy density (ΔSED) decreases over the period of 4 weeks in all treatment groups. (**C**) Sum of single treatment responses in ΔSED compared to combined treatment response, indicating antagonism, additivity, or synergism (**D**) Mean maximum SED normalized to week 20 ΔSED_{max} represented as the 99th percentile of SED values (**E**) Sum of single treatment responses in ΔSED_{max} compared to combined treatment response (**F**) Linear regression analysis between mean SED and mean SED_{max} in the trabecular region (**G**) ΔStrength in the trabecular region increases in all treatment groups (**H**) Sum of single treatment responses in ΔStrength compared to combined treatment response (**I**) Linear regression analysis of absolute strength and absolute BV/TV at week 20 (left), 22 (middle), and 24 (right).*

Table 2: Significance levels of mechanical properties*. p<0.05 as compared to the respective treatment group o: monotreatment; ● combination treatment*

Parameter	VEH	ML	BIS	BIS + ML	PTH	PTH + ML	SclAB	SclAB + ML
ΔSED [%]	oo ●●●	o ●	●●	o ●	●●	oooo	o ●	ooooo ●
ΔSED_max [%]	oooo ●●●	o ●●	o ●●	o ●●	o ●●	ooooo ●	o ●●	ooooo ●
Δeff [%]	oooo ●●●	o ●●	o ●●	o ●	o ●●	ooooo	o ●●	ooooo ●
ΔStrength [%]	oooo ●●●	o ●●	o ●●	o ●	o ●	ooo ●	o ●	ooooo ●●

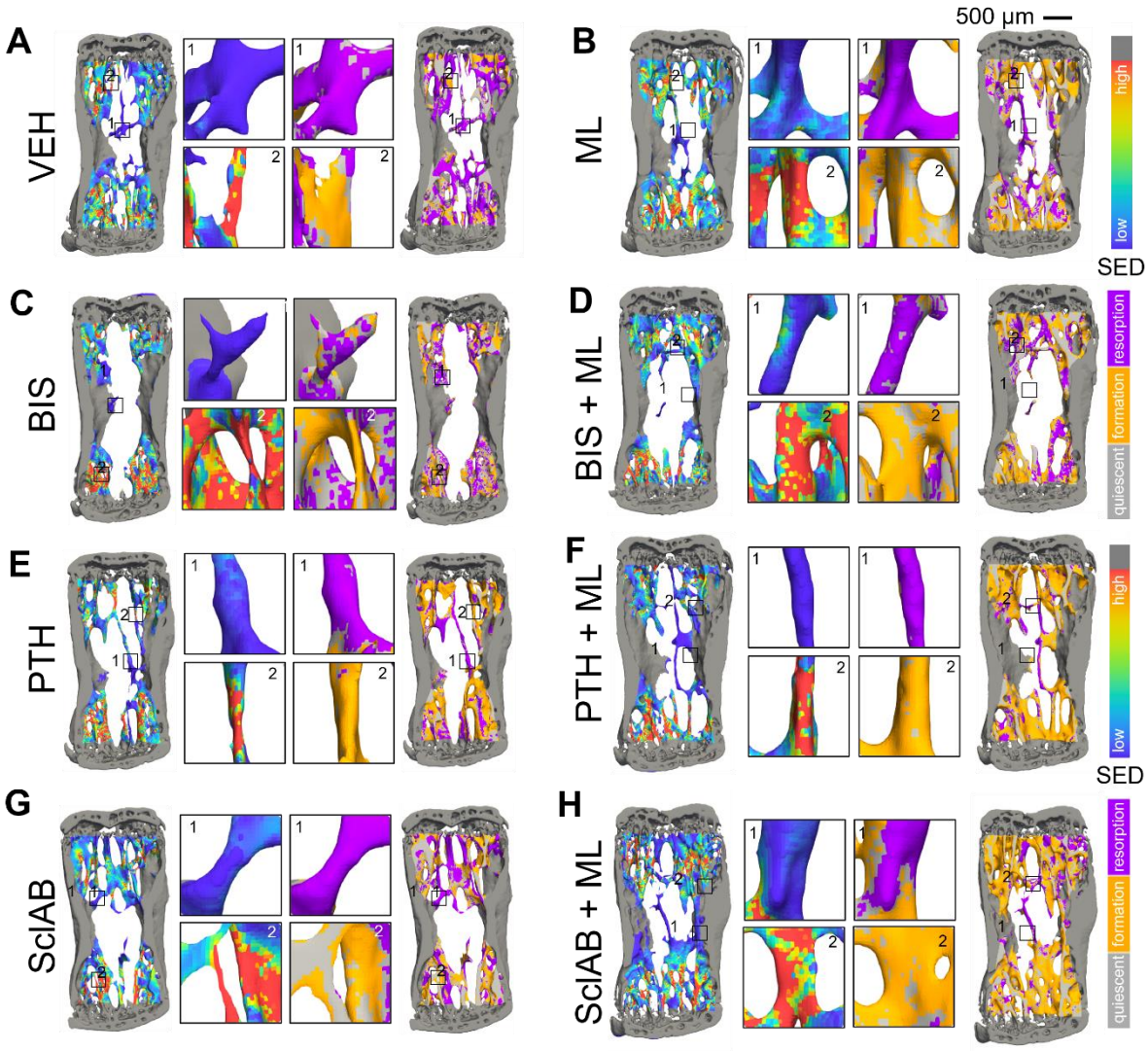

Figure 4: Formation occurs at high mechanical signal and resorption at low mechanical signal*: Three-dimensional micro-mechanical environment (SED computed with micro-finite element analysis in the basal scan) compared to trabecular bone formation and resorption sites measured with in vivo micro-computed tomography over 2 weeks. The inlet shows a magnified view of resorption (1) and formation (2) locations in individual trabeculae. Visual comparison reveals that high SED (red) matches with sites of bone formation (yellow), while low SED (blue) is predominantly found at locations of bone resorption (violet). (**A**) Slice of representative animal of the vehicle (VEH) (**B**) mechanical loading (ML) (**C**) bisphosphonate (BIS) (**D**) combined BIS + ML (**E**) parathyroid hormone (PTH), (**F**) combined PTH + ML (**G**) Sclerostin antibody (SclAB), and (**H**) combined SclAB + ML group.*

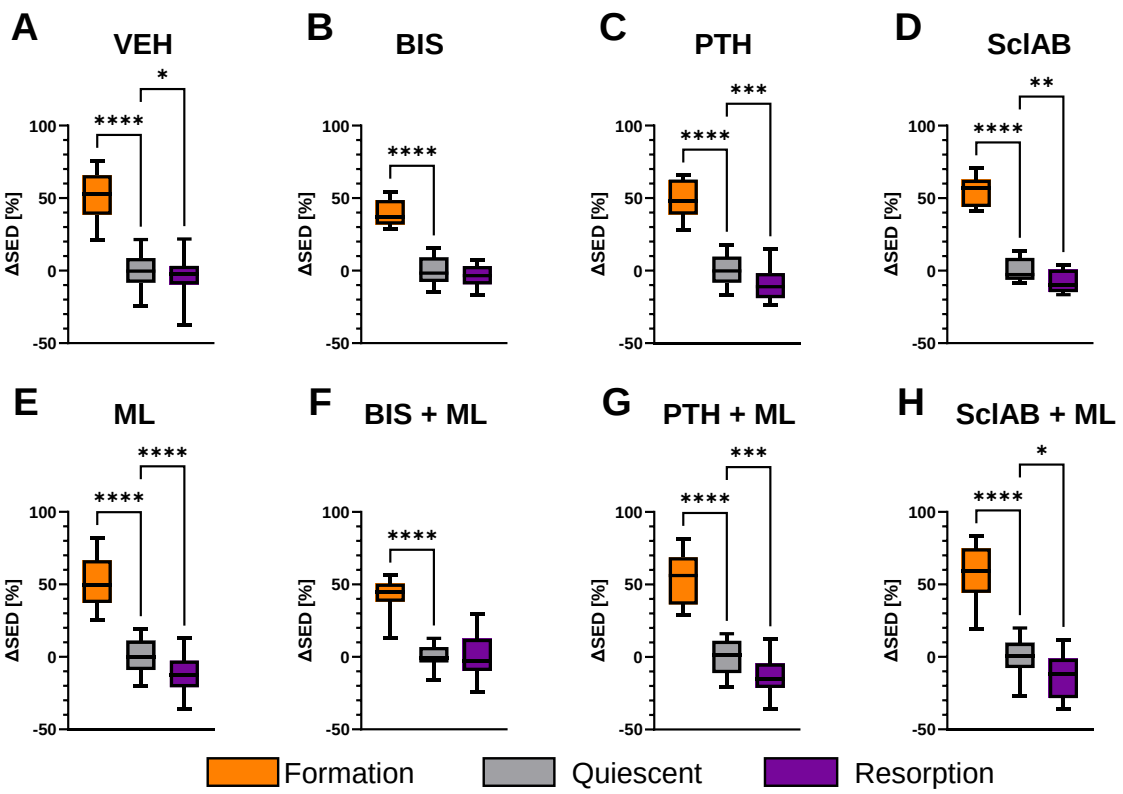

Figure 5: Mechanical signal is higher in regions of bone formation than in regions of bone resorption. *Relative differences of mean SED between quiescent, formation and resorption. SED values from the trabecular department were collected for all three remodeling events and compared to the mean SED value derived from quiescent surfaces.* ***(A)*** *Vehicle (VEH) group,* ***(B)*** *bisphosphonate (BIS) group,* ***(C)*** *parathyroid hormone (PTH) group* ***(D)*** *sclerostin antibody (SclAB) group),* ***(E)*** *mechanical loading (ML) group,* ***(F)*** *bisphosphonate and mechanical loading (BIS + ML) group,* ***(G)*** *PTH and mechanical loading (PTH + ML) group* ***(H)*** *SclAB and mechanical loading (SclAB + ML) group. Paired students t-test with Bonferroni correction; * p<0.05, ** p<0.01, *** p<0.001, **** p<0.0001*

Evidence of mechanoregulation for mono- and combined treatments

To address the question whether pharmaceutical treatments target sites in need of adaptation at the tissue level, we compared the underlying mechanical environment in the trabecular compartment with subsequent remodeling events. As can be seen in Figure 4, representative samples of each treatment group showed spatial agreement between sites of high SED and regions of subsequent bone formation, intermediate strains and sites of subsequent quiescence, and low strains and sites of subsequent resorption. To quantify this relationship, we associated remodeling events with the underlying mechanical environment obtained from micro-FE analysis by projecting SED values into volumetric clusters of bone formation. Mean SED values from formation, quiescent, and resorption volumes were calculated and normalized by mean quiescent SED of each group.

Figure 5 shows the relative mean SED differences in formed and resorbed volumes compared to quiescent clusters, quantifying the observations of Figure 4. All treatment groups showed significantly higher mean SED in formed volumes than on quiescent clusters, providing evidence of mechanoregulation in all mono- and combination treatment groups. Apart from the BIS and BIS + ML, all treatment groups demonstrated significantly lower SED values in resorbed bone volumes than in quiescent bone clusters (Fig. 5). The addition of mechanical loading to the mono-treatments resulted in marginal changes.

Mechanoregulation analysis shows differences between treatments

To quantify and compare the effects of the investigated treatments on mechanoregulation, we calculated the conditional probability curves (Figure 6 A-D), area under

the curve for the receiver operating characteristic for formation (AUC_F) and resorption (AUC_R) (Figure 6 K,L) and the correct classification rate (CCR) (Figure 6J). Mean conditional probability curves were calculated for each group event based on the clustered mechanical values for each remodeling event and fitted with exponential functions, showing the conditional probability of each remodeling event for a given surface SED value. Figure 6 E-J shows parameters of interest extracted from these curves (explained in Figure 6 I). Conditional probability plots showed that bone formation probability increased with increasing SED, and bone resorption probability decreased with decreasing SED (Figure 6 A-D).

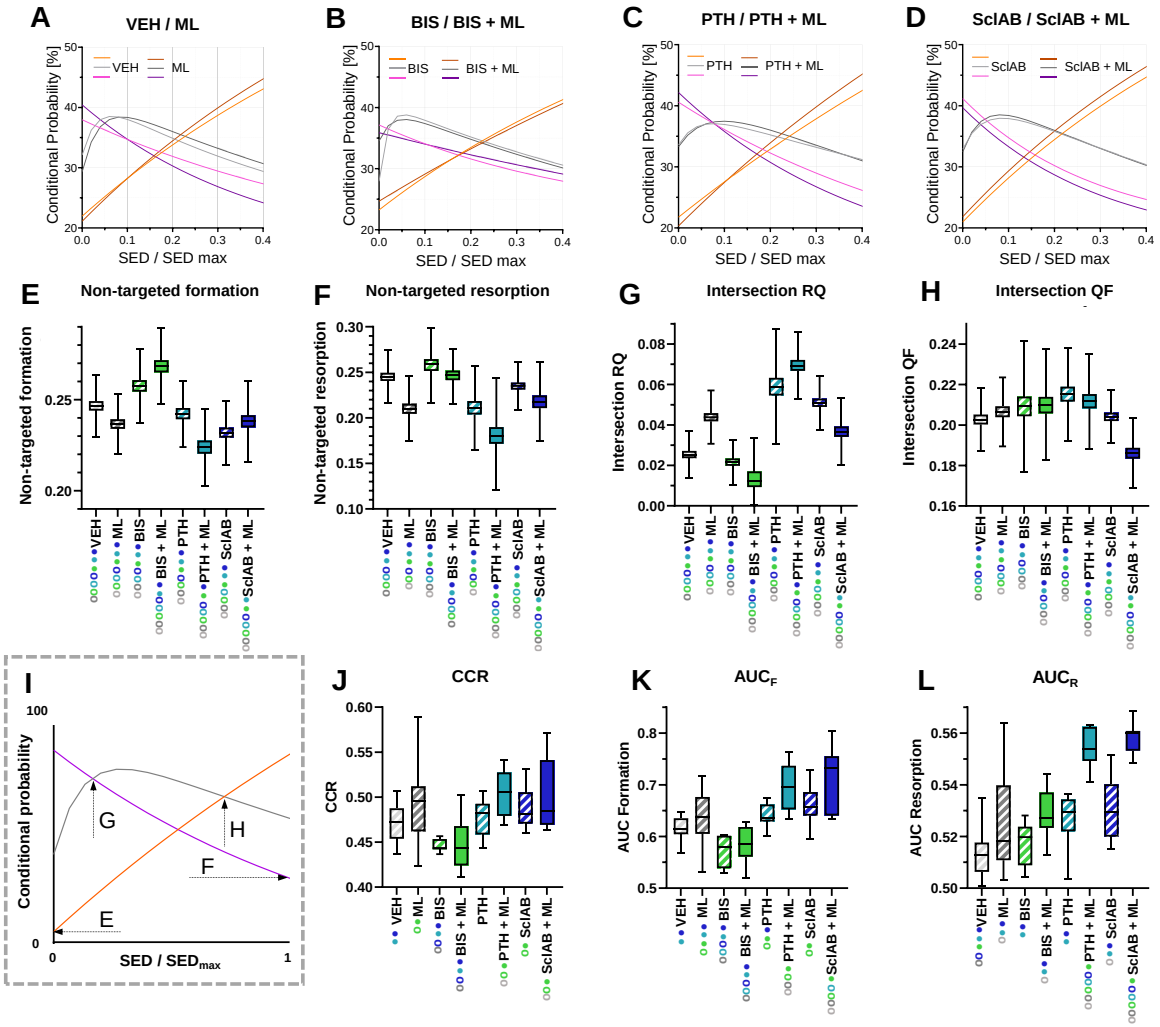

Figure 6: Conditional probabilities and quantification of mechanoregulation show differences between treatments. (A-D) *conditional probability plots,* ***(E-H)*** *points of interest from conditional probability curves, which are explained in an* ***(I)*** *example conditional probability plot,* ***(J)*** *CCR,* ***(K)*** *AUC formation,* ***(L)*** *AUC resorption. Significances were calculated with one-way Anova or Kruskal-Wallis based on normality with Tukey post-hoc-test and significant differences are depicted with a symbol in the color of the corresponding group (**o**: mono-treatment, ●:combined treatment, p<0.05)*

As expected, mechanoregulation was more pronounced in ML compared to VEH, as visualized from the conditional probability plot (Fig 6 A) where non-targeted formation (Fig 6 E) and resorption (Fig 6 F) were decreased. BIS and BIS + ML showed less mechanoregulation, as demonstrated by less steep curves in the conditional probability curves (Fig 6 B). BIS monotreatment increased non-targeted formation and resorption compared to VEH (Fig 6 E, G) resulting in the highest non-targeted resorption. Mechanical loading enhanced non-targeted formation in bisphosphonate-treated animals such that the BIS + ML group displayed the highest value for non-targeted formation.

PTH and PTH + ML conditional probability curves showed the largest change when adding mechanical loading, indicating PTH treatment benefitted most from added mechanical loading regarding mechanoregulation (Figure 6C). While PTH itself decreased non-targeted formation, the effects were less than from ML. The effects on non-targeted resorption were similar to ML. However, when adding mechanical loading to PTH, the PTH + ML group showed the lowest non-targeted formation and resorption, indicating the highest mechanoregulation among the investigated therapies.

The conditional probability plots of SclAB and SclAB + ML revealed that mechanical loading seemed to shift the formation and resorption curve up and down respectively, while not affecting the slope, meaning it mainly affected non-targeted formation and resorption (Figure 6D). SclAB monotreatment decreased non-targeted formation more than ML or PTH. It decreased non-targeted resorption, but less than ML or PTH. Adding mechanical loading to SclAB increased non-targeted formation to an extent where it was higher than ML but lower than PTH and resulted in lower non-targeted resorption compared to SclAB.

The quiescent probability curves were least affected by the treatment groups, indicating that bone strives for homeostasis. BIS + ML had the lowest resorption/quiescent intersection value (Fig. 6 G), meaning there was only a small range where resorption probability was higher than quiescent and formation. PTH + ML had the highest intersection value, where resorption was most likely to occur for the biggest SED range. Only BIS and BIS + ML decreased this value compared to VEH. Only minor changes in the intersection between the quiescent and formation conditional probability curves were observed (Figure 6H). SclAB + ML was the only treatment that decreased this value compared to VEH, meaning formation probability was dominant over the largest SED range among all treatments.

CCR values of PTH + ML (0.505) and SclAB + ML (0.504) were significantly higher than VEH (0.471), demonstrating that in order to increase overall mechanoregulation, a combination of pharmaceutical treatment and mechanical loading was necessary (Figure 6 M). BIS and BIS + ML showed significantly lower CCR values (0.447/0.448) than ML (0.491), PTH + ML, SclAB (0.487) and SclAB + ML. While SclAB monotreatment showed improved CCR values compared to BIS and BIS + ML, PTH (0.478) monotreatment did not significantly affect CCR values.

Combined treatments PTH + ML and SclAB + ML resulted in increased mechanoregulation of bone formation with AUC_F values of 0.697 and 0.711 compared to VEH (0.615), ML (0.631), BIS (0.573) and BIS + ML (0.585), but only SclAB + ML showed a significant increase over PTH monotreatment (0.642). BIS and BIS + ML resulted in the lowest AUC_F across all groups. Mechanoregulation of bone resorption, reflected in AUC_R, was increased in ML (0.525), SclAB (0.531), BIS + ML (0.529), PTH + ML (0.555) and SclAB + ML (0.558) compared to VEH (0.513) (Fig 6 O). Combined treatments PTH + ML and SclAB + ML had the greatest effect on AUC_R, with values being significantly higher than any other therapy. BIS (0.517) and PTH (0.526) monotreatment had no significant effect on AUC_R compared to VEH.

Treatments alter remodeling velocity curves and parameters

To investigate if the investigated osteoporosis treatments influence Frost's mechanostat parameters, we calculated mean remodeling velocity curves according to Marques et al. (*14*) for each treatment group (Figure 7 A-D). These curves show the net remodeling velocity for a given surface effective strain, where a negative remodeling velocity means net resorption and a positive value means net formation. Minimum and maximum remodeling velocity, as well as remodeling thresholds were extracted from the resulting curve (Figure 7 E, I, J,K). The remodeling velocity increased with increasing effective strain in all treatment groups.

Treatment generally increased remodeling velocity (Fig 7 A-D), minimum and maximum remodeling velocity (Fig 7 I, J), as well as decreased the remodeling threshold for all groups but PTH + ML (Fig 7K) compared to VEH. PTH + ML did not have a remodeling threshold as it increased the remodeling velocity especially for low strains, leading to net bone formation across the whole range of effective strain. Combined treatments generally led to increased remodeling velocities compared to monotreatments, except for BIS + ML. The remodeling velocity curves showed different effects from the investigated pharmaceutical therapies. Using VEH as the control, the remodeling velocity curve from ML was shifted up along the y-axis with a slight decrease in curvature (Figure 7A). BIS caused a remodeling velocity curve with a steep increase at low effective strain, after which the curve abruptly bent into an almost linear function with a low gradient. This effect was even more pronounced in BIS + ML. PTH increased remodeling velocity overall and decreased the curvature of the function compared to VEH/ML. PTH + ML led to an almost linear curve, except for a small increase for low effective strain. SclAB and SclAB + ML led to remodeling velocity curves that were most similar to VEH and ML and were only shifted up along the y-axis. The analysis of the minimum remodeling velocity (Figure 7I) showed that BIS + ML decreased it (-0.00585 μm/d) as compared to the respective mono-treatments (BIS: -0.00169 μm/d; ML: -0.00343 μm/d), while it was increased by the other combined treatments as compared to their respective monotreatments. VEH (-0.00837 μm/d) resulted in the lowest and PTH + ML (0.00301 μm/d) in the highest minimum remodeling velocity. The maximum remodeling velocity (Figure 7J) was highest for SclAB + ML (0.00721 μm/d), even when compared to PTH + ML (0.00676 μm/d). BIS + ML (0.000025 με) resulted in the lowest remodeling threshold, followed by SclAB + ML (0.000035 με) and BIS (0.00007 με) (not counting PTH + ML), while VEH resulted in the highest remodeling threshold (0.00105 με) (Figure 7 K).

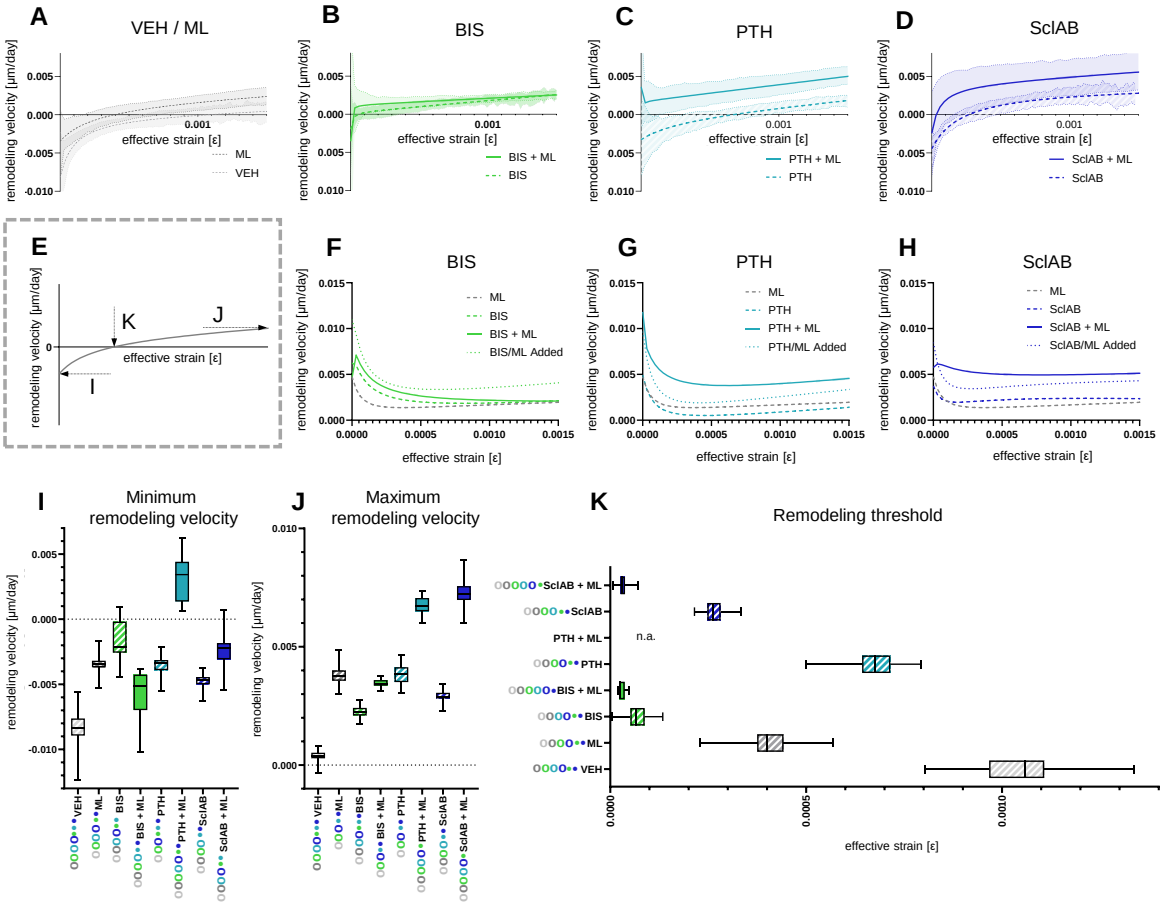

Figure 7: Remodeling velocity curves are altered by mono- and combined treatments. (A-D) *remodeling velocity curves for VEH/ML* ***(A)****, BIS* ***(B)****, PTH* ***(C)****, SclAB* ***(D)****;* ***(E)*** *example remodeling velocity curve explaining the extracted parameters in I,J and K: minimum remodeling velocity* ***(I)****, maximum remodeling velocity* ***(J)*** *and remodeling threshold (****K****) of the mechanostat curves; (F-H): treatment effects on the mechanostat curves comparing the effects of combined treatments with the respective monotreatments they consist of for BIS* ***(F)****, PTH* ***(G)****, SclAB* ***(H)****. Significances were calculated with Kruskal-Wallis test and Tukey post-hoc correction; significant differences are depicted with a symbol in the color of the corresponding group (****o****: monotreatment, ●:combined treatment, p<0.05) next to the group name*

To analyze the effects of the combined treatments in comparison to the respective monotreatments, we calculated the differences between each remodeling velocity treatment curve and the control VEH group. In order to gain a better insight into how effective a combination of treatments might be, we provided an overview of the treatment effects of the respective monotreatments, the effect of the combined treatment, and the theoretical effect of adding both monotreatment effects in Figure 7 F-H. BIS + ML showed a larger effect on remodeling velocity than ML or BIS except for very high and very low strains. However, this effect was consistently lower than the addition of the monotreatments and could thus not be considered additive. Figure 7 G shows that while PTH monotreatment increased remodeling velocity to a lesser extent than ML, the combined treatment was consistently higher than both monotreatment effects. As demonstrated in this graph, the effect of PTH + ML treatment was greatest for very low effective strain. SclAB monotreatments effects were higher than ML, and SclAB + ML combined caused a bigger effect than the addition of the effects of the monotreatments, except for <0.0001 effective strain (Fig 7 H). In contrast to PTH + ML, SclAB + ML caused a more consistent increase across all effective strain levels, as suspected by the similar shape of the SclAB + ML remodeling velocity curve compared to VEH.

How mechanoregulation affects trabecular bone mechanics

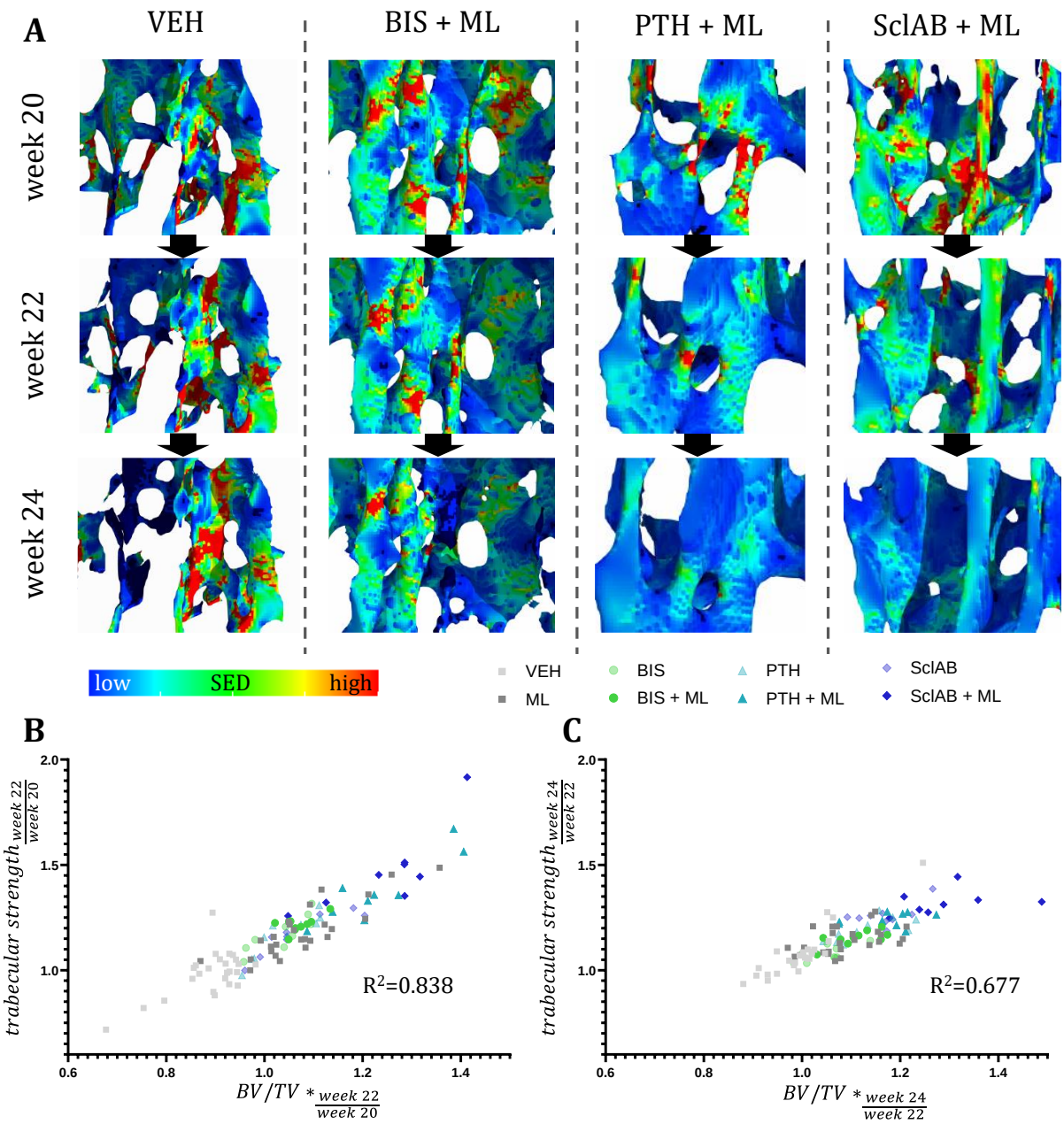

Figure 8: Mechanoregulation influences trabecular strength. (A) *Qualitative comparison of SED distribution for VEH, BIS + ML, PTH + ML and SclAB.* ***(B,C)*** *Adjusted ratio of BV/TV over time with CCR as a measure of mechanoregulation correlated with the ratio of trabecular strength over time for* ***(B)*** *week 20-22 and* ***(C)*** *week 22-24*

Finally, we analyzed how mechanoregulation can affect global trabecular mechanics of the bone (Figure 8). We adjusted the ratio of BV/TV for mechanoregulation using CCR, which indicates how much bone remodeling is targeted to the mechanical demands (BV/TV*). Figure 8A shows how the SED distribution in trabecular bone changed over time in the three combined treatments and the control VEH. In the VEH group, in several areas high SED values decreased over time, but in other areas they increase. Additionally, Figure 8A illustrates how the resorption of a single trabecula leads to a more heterogeneous SED distribution. While SED on average decreased over time for BIS + ML, this did not particularly affect areas with high SED, as there still remained some in week 24. In contrast, both PTH + ML and SclAB + ML showed large decreases in SED, especially in areas with high SED values in week 20. Figure 8B and C show the correlation of CCR-adjusted BV/TV (BV/TV*) with the change in trabecular strength for week 20-22 and 22-24 respectively. In week 20-22 a strong correlation between

BV/TV* and change in trabecular strength (R^2= 0.794) was found, with VEH demonstrating the lowest values for both parameters and PTH + ML and SclAB + ML demonstrating the highest values for both parameters (Fig 8B). BIS and BIS + ML samples largely overlapped, while mechanical loading showed an obvious shift in the other treatment groups. Although we still found a positive correlation between BV/TV* and change in trabecular strength in week 22-24, this was less pronounced than in the previous time span. While our results indicate that increased mechanoregulation may lead to a decrease in high strain values and increased trabecular strength, they also suggest a time dependency of the combined treatments.

DISCUSSION

Include a Discussion that summarizes your conclusions and elaborates on their implications. There should be a paragraph outlining the limitations of your results and interpretation, as well as a discussion of the steps that need to be taken for the findings to be applied in the clinic. Please avoid claims of priority and avoid repeating the conclusions at the end.

In this study, the effects of combining mechanical loading with current pharmaceutical osteoporosis treatments (BIS, PTH or SclAB) were investigated in a mouse model of osteoporosis. Our findings suggest that combining mechanical loading with anabolic pharmaceutical treatments leads to improved effects on bone morphometric parameters and mechanoregulation compared to the respective monotreatments. Although bisphosphonate treatment was not impaired by combination with mechanical loading, it failed to recover the deleterious effects of bisphosphonates on mechanoregulation. While sclerostin antibody treatment and PTH treatment showed synergistic effects when combined with mechanical loading, PTH treatment benefitted most from mechanical loading, indicated by increased CCR and AUC_F compared to monotreatment.

PTH led to increases in trabecular bone volume fraction, with our results suggesting that this could be at the cost of trabecularization of the endocortical surface (Fig. 1E). In line with our findings, Meakin et al. reported a marked increase in cortical porosity which loading reduced (*18*). Our data showed increased MS but contrary to existing literature also decreased ES in the second time window, and combined with mechanical loading, the observed effects were even more pronounced. A reason for this discrepancy could be the different measurement method of *in vivo* dynamic morphometry which allows transient non-invasive assessment of bone formation and resorption, having to be considered for the assessment of bone resorption. Furthermore, PTH has been reported to act site-specifically and dose-specifically, also having to be considered for potential differences amongst research findings.

We found increased sensitivity of mechanoregulation mechanisms for PTH combined with mechanical loading but not for only PTH (Figure 6), which is in line with the results of Ryder et al, where PTH combined with fluid flow increased the mechanoresponse of osteoblasts (*22*), although PTH alone did not. Hagino et al. hypothesized that PTH lowers the remodeling threshold of the remodeling velocity function, which we were able to confirm (*23*) (Figure 7). Notably, combining PTH with mechanical loading lowered the remodeling threshold to such an extent that the entire remodeling velocity curve was positive, meaning that even for very low effective strain, there is more formation than resorption, leading to net bone formation. These results are in agreement with data from studies by Miller et al., where the effects of PTH + ML resulted in an overall increase of cortical thickness at zero longitudinal strain, and effects varied for different surface strains, suggesting altered mechanoregulation (*24*).

In the current study, sclerostin antibody treatment resulted in a synergistic increase in bone mass and strength when combined with mechanical loading. Bone formation rates were

increased, and bone resorption rates were decreased as compared to single treatments. Sclerostin antibodies alone or in combination with mechanical loading both led to increased mechanoregulation, showing similar curve characteristics for conditional probabilities and remodeling velocities. It has been suggested that the decoupling of bone formation and resorption caused by sclerostin antibodies is similar to the effect of mechanical loading, to the extent of being interchangeable (*25*). While mechanical loading also uses sclerostin-independent pathways (*26*), our static, dynamic, mechanoregulation analysis suggests that sclerostin antibody treatment affects bone remodeling in a similar way. However, Morse et al. reported sclerostin antibody treatment combined with mechanical loading affected different genes related to the Wnt/β-catenin pathway (*19*), which could be a reason for a synergistic response elicited by the combination on the remodeling velocity curve. Occurring synergisms might be explained by the interplay between factors other than sclerostin in the mechanical response to loading. One candidate could be the Dickkopf-1 (Dkk1) protein which when inhibited in combination with sclerostin, resulted in a robust osteoanabolic effect in mice (*27*).

Bisphosphonates were the only treatment that preserved Tb.N compared to all other groups. Clinical studies on postmenopausal women found no effects of combination treatment (*28*), with differences of bisphosphonate treatment alone depending on the bone and site (*29*), while Kistler-Fischbacher et al. found positive effects of bisphosphonate and mechanical loading treatment in the load-bearing femoral neck which were less pronounced in the spine, and also dependent on the kind of exercise (*30*). Stadelmann et al. found additive effects on cortical thickness for several areas, however, bisphosphonates seemed to impair mechanical loading in regions of high strains (*31*), which suggested altered mechanosensation. In trabecular bone, Sugiyama et al. found that no improvements of combining bisphosphonates and mechanical loading in trabecular bone of mouse tibia (*16*). This corroborates our finding of decreased mechanoregulation under bisphosphonate treatment (Fig. 6F), which could not be recovered by additional mechanical loading and showed that bisphosphonates decreased bone formation where it was mechanically most needed (Fig. 7 J). Since mineralized and eroded surface were similar in the bisphosphonate group compared to the vehicle group, our results suggest that bisphosphonates not only affect the activity of osteoclasts but also the mechanosensitivity of osteoblasts. Namely, the coupling process between osteoclasts and osteoblasts could be disturbed by osteoclast apoptosis (*32*). Additionally, bisphosphonates impair osteoblast activation (*33*), likely affecting spatial distribution, where cells are less guided by the mechanical signal.

By adjusting the ratio of BV/TV for mechanoregulation using CCR, we were able to show a strong positive correlation with the change in trabecular strength calculated with the Pistioa criterion, implying that when mechanoregulation increases, the amount of high local SED values decrease. Regions with high local strain are linked to higher occurrences of microscopic tissue damage (*34*), of which even small amounts can cause large reductions in strength (*35*) and increase fracture risk (*36*). While BV/TV is a known estimator of bone mechanical performance (*35*), we show that increased sensitivity of mechanoregulation parameters could help decrease fatigue fracture risk. Cosman et al. (*37*) reported a decrease in vertebral fractures after monthly sclerostin antibody treatment in postmenopausal women, where fatigue fractures are common (*38*), but not in other bones. This supports our conclusion, that sclerostin-antibody-induced increases in mechanoregulation can help decrease fatigue fracture risk.

Clearly, the use of mice as a model for human skeletal metabolism has its limitations. While our results suggest that mechanical loading is of importance for therapeutic success, clinical studies will be required to determine whether this can be translated to humans through specific types of physical activity. A growing body of studies reports site specific differences in therapeutic effects. All experiments in the present study were performed using young mice

which responded well to incoming mechanical demands while it has been shown that mechanoresponsiveness decreases with increasing age (*4*).

With regard to future translational studies, exercise-based loading programs might represent a relevant clinical scenario where pharmaceutical and physical therapies are combined in order to exploit the potential of the synergistic effects of mechanical loading and anabolic pharmaceutical treatments. As was found in the FRAME clinical trial, bone-forming effects of Romosozumab, a clinical version of sclerostin antibodies, on periosteal surfaces may require mechanical loading and potentially only manifest themselves in weight-bearing sites (*39*). Furthermore, 12 months resistance or jump training as well as running a marathon reportedly decreased sclerostin levels (*40*, *41*).

While many studies focus on pharmaceutical treatments, few investigate the therapeutic potential of mechanical loading in the form of load-bearing exercise. Our results indicate that mechanical loading has a strong positive effect on anabolic osteoporosis treatments without impacting the effectiveness of anti-resorptive treatments. Similarly as finding a suitable dose regimen with pharmaceuticals, optimizing targeted kinds of exercise protocols is a necessary requirement given that treatment outcome is dependent on the type of exercise performed. Our analysis of mechanoregulation also demonstrates the potential of sclerostin antibodies and the combined treatments of sclerostin antibodies or PTH together with mechanical loading on bone formation and targeting morphometric effects to the mechanical needs of the bone. While current studies mostly investigate treatment-induced changes to static bone morphometry, our results suggest that in the future, more attention needs to be paid to mechanical parameters, e.g. using the capabilities of FE modelling to simulate load transfer to further our understanding of the mechanisms behind bone adaptation.

In conclusion, our discovery of robust anabolic effects of combined mechanical loading and anabolic pharmaceutical agents in trabecular bone suggests that osteoporosis patients would benefit greatly from a combined pharmaceutical and physical therapy plan. Combining PTH or sclerostin antibody treatment with mechanical loading not only results in increased bone formation, but also increases the sensitivity of mechanoregulation parameters, ensuring that anabolic effects in trabecular bone are more targeted to the mechanical needs. Mechanical loading combined with pharmaceutical therapy may therefore offer physicians an additional treatment option for patients with low bone mass who are still physically active.

MATERIALS AND METHODS

Study design

The study design is illustrated in Figure 1A. In total, 120 female 15-week-old C57Bl/6J mice (RCC, Füllinsdorf, Switzerland) were subjected to bilateral ovariectomy. A basal micro-computed tomography (micro-CT) image of the 6th caudal vertebra was obtained (Scanco Medical, Brüttisellen, Switzerland). Recovery lasted five weeks after surgery, as in this period, an osteopenic state was established in the trabecular compartment of the 6th caudal vertebra in a previous study (*42*). Pinning of the adjacent vertebrae as preparation for the loading procedure took place in week 17. At week 20, the animals were divided into 8 groups and the following treatments were administered for the following four weeks: BIS (n=9), BIS + ML (n=10), PTH (n=10), PTH + ML (n=9), SclAB (n=9), SclAB+ML (n=8), ML (n=26), VEH (n=25). In the SclAB study, 4 mice showed a periosteal reaction, possibly due to injury of the periosteum during intravenous injection at the tail vein. 10 mice were excluded due to swollen tails or loose

pins. These mice were excluded from evaluation, resulting in 106 animals included. Micro-computed tomography was performed in weeks 15, 20, 22 and 24. Surgeries, imaging, and loading were performed under isoflurane anesthesia (induction 4%, maintenance 1.5-2.5%, Attane, Piramal Healthcare, India). Vehicle control was an isotonic buffer (pH 5.3).

After the experiment, the mice were sacrificed. While the data was gained in three experiments (at different times), study and loading parameters were not different except for the administered pharmaceutical treatments, thus combined in this study. ML and VEH groups from all experiments were merged, explaining the larger sample size in these groups. All animal experiments were performed with approval of the local authority (Kantonales Veterinäramt Zürich, Zürich, Switzerland).

Mechanical loading

To induce a bone response under controlled loading conditions, we used a mouse tail loading model which permits the study of trabecular bone adaptation in vivo (*42-44*). Specifically, three weeks before loading start, pins were inserted into the 5th and 7th caudal vertebra under fluoroscopic control. At start of mechanical loading, the 6th caudal vertebra (CV6) was subjected to cyclic mechanical loading at a force of 8 N delivered through a specifically designed CVAD loading device, 3 times/week for 4 weeks at 10 Hz and 3000 cycles. Control groups received the same pins into the 5th and 7th vertebrae, were mounted into the mechanical CVAD loading device and were given the same amount of anesthesia for a period equivalent to the loading group; however, no force was applied to the vertebra.

Pharmaceutical treatment

In the BIS groups, a dose of 100 µg/kg zolendronate (Zometa 4mg/5ml; Novartis Pharma Schweiz AG, Bern) was administered once in week 20. The zolendronate was diluted with 0.9 % NaCl. Vehicle consisted of 0.9 % NaCl, was injected subcutaneously once in week 20.

In the PTH groups, a daily dose of 40 µg/kg of PTH (hPTH 1-34, Bachem AG, Switzerland) or vehicle was injected over 4 weeks. The PTH was dissolved in 0.9% NaCl (0.9% Natriumchloridlösung, B. Braun Medical AG, Switzerland) and 2% heat inactivated mouse serum (Immundiagnostik AG, Bensheim, Germany). The vehicle consisted of 0.9% NaCl, heat inactivated mouse serum and HCl to adjust the pH. In the SclAB groups, a weekly dose of 100mg/kg, 5ml i.v./kg BW SclAB (Novartis Pharma AG, Basel, Switzerland) was administered over 4 weeks.

Imaging and image processing

The detailed imaging and image processing methods are provided in the supplementary material.

Static and dynamic bone morphometry

Static trabecular bone morphometric parameters were calculated according to Bouxsein et al. (*45*). Because of the large amount of data accumulated in this study we will focus on the most relevant parameters in this article, bone volume fraction (BV/TV) of the trabecular compartment, trabecular thickness (Tb.Th) and trabecular number (Tb.N). Dynamic bone morphometry was performed by registering and superimposing segmented bone volume images of consecutive time points. Bone formation and resorption rates were calculated as described

previously (*46*). Dynamic parameters were calculated over two two-week periods (week 20-22 and week 22-24).

Analysis of mechanical parameters

Finite-element simulations were used to analyze mechanical properties of the vertebrae. The detailed finite-element methods are provided in the supplementary material. Strain energy density (SED), defined as the increase in energy associated with the tissue deformation per unit volume, and effective strain (*47*) were used as the mechanical signal. Trabecular bone strength was estimated for each mouse at each time point by using the Pistoia criterion (*48*) which assumes that bone failure is initiated if a certain percentage of the bone tissue (2%) is strained beyond the tissue yield strain (7000 με). For the trabecular strength estimation, the full bone was modeled but only the strains in the trabecular compartment were analyzed.

Analysis of local mechanoregulation

To associate sites of formation or resorption with the local mechanical environment on the trabecular bone surface, the mechanical environment at time 20 weeks was projected into the volumetric formation and resorption clusters, at week 20 to 22 using the method published by Griesbach et al. (*15*). The two volumetric clusters for formation and resorption as well as the quiescent surface of the superimposed micro-CT scans were used as masks and applied to the SED image. Mean SED values from these clusters were calculated and normalized by mean quiescent SED of each group (*3*). Area under the curve for the receiver operating characteristic were calculated for formation (AUC_F) and resorption (AUC_R) based on the respective clustered mechanical values and the mechanical values on the bone surface (*15, 44*).

Conditional probabilities were calculated for each remodeling based on the remodeling clusters (*3*). First, histograms with 50 bins were created for formation, quiescence and resorption, and consequently rescaled to contain the same amount of values to remove dependencies on imbalances in the remodeling process due to differences between animals or treatments. Conditional probabilities were obtained by bin-wise division of the rescaled histograms by the sum of the three remodeling histograms.

Mean conditional probabilities were calculated for all animals within one group and fitted with exponential functions. To compare parameters extracted from these functions, a bootstrapping approach was used by creating 2500 subsamples from each group (*14, 49*), fitting the conditional probability functions to the mean curve of each subsample. For formation and resorption, the minimum probability, indicating the amount of non-targeted formation or resorption, were compared between groups. Additionally, the intersections between the resorption and quiescent curve, and the quiescent and formation curve were computed. Furthermore, CCR values were calculated from the mean conditional probabilities from all animals, returning a scalar value between 0.33 and 1 assessing overall mechanoregulation, with 0.33 meaning remodeling is independent of the mechanical signal and 1 meaning it is entirely dependent on the mechanical signal.

Analysis of remodeling velocities

(Re)modeling velocities and their mechanostat parameters were calculated according to Marques et al. for each animal (*14*). As treatments altered the curve characteristics (Figure 7), we extended the hyperbolic curve fit used by Marques et al. by adding a linear component $RmV(x) = y_0 - \frac{a}{b*x} + c * x$ and fitted it to the mean remodeling velocity curve for each group.

Minimum and maximum remodeling velocity, as well as remodeling thresholds were extracted from the resulting curve. To enable statistical comparison of parameters derived from the curve fits, we used a bootstrapping approach creating 2500 subsamples from each group and fitting the extended hyperbolic function to the mean remodeling velocity curve of each subsample (*14, 49*). In order to compare treatment effects, we subtracted each remodeling velocity curve with the control remodeling velocity curve for the VEH group. The result represented the respective treatment effect on the remodeling velocity over the relevant effective strain values for each group. Additionally, we added the treatment effect of each pharmaceutical treatment to the effect of the ML group, to use as a reference of comparison for the combined treatment and assess and visualize if the effect was additive or even synergistic (*24*).

Correlation of mechanoregulation, BV/TV and mechanical properties

To investigate the effects of mechanoregulation on global mechanical properties we adjusted the ratio of BV/TV (e.g. $BV/TV_{week\ 22}$ /$BV/TV_{week\ 20}$) to account for mechanoregulation using the square root of CCR (BV/TV*). Additionally, CCR was divided by the average result for the VEH group (0.47), to obtain a value in a similar range as BV/TV. While BV/TV includes all bone remodeling, BV/TV* indicates how much bone remodeling is targeted to the mechanical demands. We then correlated BV/TV* with the change in trabecular strength (e.g. trabecular $strength_{week\ 22}$ /trabecular $strength_{week\ 20}$) for each animal and time interval across all groups. R^2 was reported for both time intervals.

Statistical methods

Morphometric parameters were normalized to treatment start (week 20) for each animal. For the effect of ovariectomy, statistical analysis was performed using one-way ANOVA. Static, dynamic, and mechanical treatment effects were compared using two-way ANOVA over time and group with Tukey post-hoc-test. Synergism was defined as when the combined treatment excessed the sum of the two single treatments and additivity was defined as when the combined treatment was equal to the sum of the two single treatments. Comparison of parameters of the mechanoregulation and the mechanostat analysis was performed using Kruskal-Wallis-Test with Tukey post-hoc test. Correlations were assessed with Pearson's coefficient and R^2. Statistical analysis was performed using R (R, Auckland, New Zealand, (*50*) and GraphPad Prism 10 software. Data are presented as mean ± standard deviation unless otherwise specified. P-values lower than 0.05 are considered significant.

Acknowledgments

We acknowledge Kathleen Koch for assistance and performance of animal experiments of the PTH and BIS groups, and Dr. Ulrike Kettenberger for assistance and performance of animal experiments of the PTH group. Finite element simulations were performed on the Euler cluster operated by Scientific IT Services at ETH Zurich.

Funding:

European Union grant VPHOP FP7-ICT-2008-223865 (FS, FML, GK, CW)

Author contributions:

Conceptualization: RM, GAK, PJR

Methodology: CW, GAK, MS, FML
Investigation: JG, FAS, CW, MS, FML, GAK, FCM
Visualization: FAS, JG
Funding acquisition: RM, GAK
Project administration: GAK, RM
Supervision: RM, GAK, PJR
Writing – original draft: FAS, JG
Writing – review & editing: CW, MS, FML, FCM, PJR, MK, GAK, RM

Competing interests:

M.K. and P.R. are employees of Novartis. The other authors declare they have no competing interests.

Data and materials availability: All data are available in the main text or the supplementary materials.

References

1. H. M. Frost, Bone "mass" and the "mechanostat": a proposal. *Anat Rec* **219**, 1-9 (1987).
2. H. M. Frost, Bone's mechanostat: a 2003 update. *Anat Rec A Discov Mol Cell Evol Biol* **275**, 1081-1101 (2003).
3. F. A. Schulte, D. Ruffoni, F. M. Lambers, D. Christen, D. J. Webster, G. Kuhn, R. Muller, Local mechanical stimuli regulate bone formation and resorption in mice at the tissue level. *PLoS One* **8**, e62172 (2013).
4. H. Razi, A. I. Birkhold, R. Weinkamer, G. N. Duda, B. M. Willie, S. Checa, Aging Leads to a Dysregulation in Mechanically Driven Bone Formation and Resorption. *J Bone Miner Res* **30**, 1864-1873 (2015).
5. P. Christen, K. Ito, R. Ellouz, S. Boutroy, E. Sornay-Rendu, R. D. Chapurlat, B. van Rietbergen, Bone remodelling in humans is load-driven but not lazy. *Nat Commun* **5**, 4855 (2014).
6. M. Walle, F. C. Marques, N. Ohs, M. Blauth, R. Muller, C. J. Collins, Bone Mechanoregulation Allows Subject-Specific Load Estimation Based on Time-Lapsed Micro-CT and HR-pQCT in Vivo. *Front Bioeng Biotechnol* **9**, 677985 (2021).
7. D. B. Burr, Targeted and nontargeted remodeling. *Bone* **30**, 2-4 (2002).
8. J. M. Graham, B. P. Ayati, S. A. Holstein, J. A. Martin, The role of osteocytes in targeted bone remodeling: a mathematical model. *PLoS One* **8**, e63884 (2013).
9. J. A. Kanis, E. V. McCloskey, H. Johansson, A. Oden, L. J. Melton, N. Khaltaev, A reference standard for the description of osteoporosis. *Bone* **42**, 467-475 (2008).
10. K. W. Lyles, C. S. Colón-Emeric, J. S. Magaziner, J. D. Adachi, C. F. Pieper, C. Mautalen, L. Hyldstrup, C. Recknor, L. Nordsletten, K. A. Moore, C. Lavecchia, J. Zhang, P. Mesenbrink, P. K. Hodgson, K. Abrams, J. J. Orloff, Z. Horowitz, E. F. Eriksen, S. Boonen, Zoledronic acid and clinical fractures and mortality after hip fracture. *New Engl J Med* **357**, 1799-1809 (2007).
11. R. Baron, M. Kneissel, WNT signaling in bone homeostasis and disease: from human mutations to treatments. *Nat Med* **19**, 179-192 (2013).
12. I. Hoffmann, M. Kohl, S. von Stengel, F. Jakob, K. Kerschan-Schindl, U. Lange, S. Peters, D. Schoene, C. Sieber, F. Thomasius, H. A. Bischoff-Ferrari, M. Uder, W. Kemmler, Exercise and the prevention of major osteoporotic fractures in adults: a systematic review and meta-

analysis with special emphasis on intensity progression and study duration. *Osteoporos Int* **34**, 15-28 (2023).

13. R. B. Choi, A. G. Robling, The Wnt pathway: An important control mechanism in bone's response to mechanical loading. *Bone* **153**, 116087 (2021).
14. F. C. Marques, D. Boaretti, M. Walle, A. C. Scheuren, F. A. Schulte, R. Müller, Mechanostat parameters estimated from time-lapsed micro-computed tomography data of mechanically driven bone adaptation are logarithmically dependent on loading frequency. *Front Bioeng Biotech* **11**, (2023).
15. J. K. Griesbach, F. A. Schulte, G. N. Schadli, M. Rubert, R. Muller, Mechanoregulation analysis of bone formation in tissue engineered constructs requires a volumetric method using time-lapsed micro-computed tomography. *Acta Biomater*, (2024).
16. T. Sugiyama, L. B. Meakin, G. L. Galea, B. F. Jackson, L. E. Lanyon, F. H. Ebetino, R. G. Russell, J. S. Price, Risedronate does not reduce mechanical loading-related increases in cortical and trabecular bone mass in mice. *Bone* **49**, 133-139 (2011).
17. T. Sugiyama, L. K. Saxon, G. Zaman, A. Moustafa, A. Sunters, J. S. Price, L. E. Lanyon, Mechanical loading enhances the anabolic effects of intermittent parathyroid hormone (1-34) on trabecular and cortical bone in mice. *Bone* **43**, 238-248 (2008).
18. L. B. Meakin, H. Todd, P. J. Delisser, G. L. Galea, A. Moustafa, L. E. Lanyon, S. H. Windahl, J. S. Price, Parathyroid hormone's enhancement of bones' osteogenic response to loading is affected by ageing in a dose- and time-dependent manner. *Bone* **98**, 59-67 (2017).
19. A. Morse, A. Schindeler, M. M. McDonald, M. Kneissel, I. Kramer, D. G. Little, Sclerostin Antibody Augments the Anabolic Bone Formation Response in a Mouse Model of Mechanical Tibial Loading. *J Bone Miner Res* **33**, 486-498 (2018).
20. S. T. Robinson, P. T. Shyu, X. E. Guo, Mechanical loading and parathyroid hormone effects and synergism in bone vary by site and modeling/remodeling regime. *Bone* **153**, 116171 (2021).
21. F. M. Lambers, F. A. Schulte, G. Kuhn, D. J. Webster, R. Muller, Mouse tail vertebrae adapt to cyclic mechanical loading by increasing bone formation rate and decreasing bone resorption rate as shown by time-lapsed in vivo imaging of dynamic bone morphometry. *Bone* **49**, 1340-1350 (2011).
22. K. D. Ryder, R. L. Duncan, Parathyroid hormone modulates the response of osteoblast-like cells to mechanical stimulation. *Calcif Tissue Int* **67**, 241-246 (2000).
23. H. Hagino, T. Okano, M. P. Akhter, M. Enokida, R. Teshima, Effect of parathyroid hormone on cortical bone response to in vivo external loading of the rat tibia. *J Bone Miner Metab* **19**, 244-250 (2001).
24. C. J. Miller, S. Trichilo, E. Pickering, S. Martelli, E. Dall'Ara, P. Delisser, L. B. Meakin, P. Pivonka, Cortical thickness adaptation to combined mechanical loading and parathyroid hormone treatments is site specific and synergistic in the mouse tibia model. *Bone* **180**, 116994 (2024).
25. T. Sugiyama, T. Torio, T. Miyajima, Y. T. Kim, H. Oda, Romosozumab and blosozumab: alternative drugs of mechanical strain-related stimulus toward a cure for osteoporosis. *Front Endocrinol (Lausanne)* **6**, 54 (2015).
26. A. Morse, M. M. McDonald, N. H. Kelly, K. M. Melville, A. Schindeler, I. Kramer, M. Kneissel, M. C. van der Meulen, D. G. Little, Mechanical load increases in bone formation via a sclerostin-independent pathway. *J Bone Miner Res* **29**, 2456-2467 (2014).
27. P. C. Witcher, S. E. Miner, D. J. Horan, W. A. Bullock, K. E. Lim, K. S. Kang, A. L. Adaniya, R. D. Ross, G. G. Loots, A. G. Robling, Sclerostin neutralization unleashes the osteoanabolic effects of Dkk1 inhibition. *JCI Insight* **3**, (2018).
28. K. Uusi-Rasi, P. Kannus, S. Cheng, H. Sievanen, M. Pasanen, A. Heinonen, A. Nenonen, J. Halleen, T. Fuerst, H. Genant, I. Vuori, Effect of alendronate and exercise on bone and physical performance of postmenopausal women: a randomized controlled trial. *Bone* **33**, 132-143 (2003).
29. P. D. Chilibeck, K. S. Davison, S. J. Whiting, Y. Suzuki, C. L. Janzen, P. Peloso, The effect of strength training combined with bisphosphonate (etidronate) therapy on bone mineral, lean tissue, and fat mass in postmenopausal women. *Can J Physiol Pharmacol* **80**, 941-950 (2002).

30. M. Kistler-Fischbacher, J. S. Yong, B. K. Weeks, B. R. Beck, A Comparison of Bone-Targeted Exercise With and Without Antiresorptive Bone Medication to Reduce Indices of Fracture Risk in Postmenopausal Women With Low Bone Mass: The MEDEX-OP Randomized Controlled Trial. *J Bone Miner Res* **36**, 1680-1693 (2021).
31. V. A. Stadelmann, N. Bonnet, D. P. Pioletti, Combined effects of zoledronate and mechanical stimulation on bone adaptation in an axially loaded mouse tibia. *Clin Biomech (Bristol, Avon)* **26**, 101-105 (2011).
32. N. A. Sims, T. J. Martin, Osteoclasts Provide Coupling Signals to Osteoblast Lineage Cells Through Multiple Mechanisms. *Annu Rev Physiol* **82**, 507-529 (2020).
33. P. R. Jensen, T. L. Andersen, P. Chavassieux, J. P. Roux, J. M. Delaisse, Bisphosphonates impair the onset of bone formation at remodeling sites. *Bone* **145**, (2021).
34. M. G. Goff, F. M. Lambers, R. M. Sorna, T. M. Keaveny, C. J. Hernandez, Finite element models predict the location of microdamage in cancellous bone following uniaxial loading. *J Biomech* **48**, 4142-4148 (2015).
35. C. J. Hernandez, F. M. Lambers, J. Widjaja, C. Chapa, C. M. Rimnac, Quantitative relationships between microdamage and cancellous bone strength and stiffness. *Bone* **66**, 205-213 (2014).
36. F. M. Lambers, A. R. Bouman, C. M. Rimnac, C. J. Hernandez, Microdamage caused by fatigue loading in human cancellous bone: relationship to reductions in bone biomechanical performance. *PLoS One* **8**, e83662 (2013).
37. F. Cosman, D. B. Crittenden, J. D. Adachi, N. Binkley, E. Czerwinski, S. Ferrari, L. C. Hofbauer, E. Lau, E. M. Lewiecki, A. Miyauchi, C. A. Zerbini, C. E. Milmont, L. Chen, J. Maddox, P. D. Meisner, C. Libanati, A. Grauer, Romosozumab Treatment in Postmenopausal Women with Osteoporosis. *N Engl J Med* **375**, 1532-1543 (2016).
38. T. M. Keaveny, E. F. Wachtel, D. L. Kopperdahl, Mechanical behavior of human trabecular bone after overloading. *J Orthop Res* **17**, 346-353 (1999).
39. E. F. Eriksen, R. Chapurlat, R. W. Boyce, Y. Shi, J. P. Brown, S. Horlait, D. Betah, C. Libanati, P. Chavassieux, Modeling-Based Bone Formation After 2 Months of Romosozumab Treatment: Results From the FRAME Clinical Trial. *J Bone Miner Res* **37**, 36-40 (2022).
40. P. S. Hinton, P. Nigh, J. Thyfault, Serum sclerostin decreases following 12 months of resistance- or jump-training in men with low bone mass. *Bone* **96**, 85-90 (2017).
41. K. Kerschan-Schindl, M. M. Thalmann, E. Weiss, M. Tsironi, U. Foger-Samwald, J. Meinhart, K. Skenderi, P. Pietschmann, Changes in Serum Levels of Myokines and Wnt-Antagonists after an Ultramarathon Race. *PLoS One* **10**, e0132478 (2015).
42. F. M. Lambers, G. Kuhn, F. A. Schulte, K. Koch, R. Muller, Longitudinal assessment of in vivo bone dynamics in a mouse tail model of postmenopausal osteoporosis. *Calcif Tissue Int* **90**, 108-119 (2012).
43. D. J. Webster, P. L. Morley, G. H. van Lenthe, R. Muller, A novel in vivo mouse model for mechanically stimulated bone adaptation--a combined experimental and computational validation study. *Comput Methods Biomech Biomed Engin* **11**, 435-441 (2008).
44. A. C. Scheuren, P. Vallaster, G. A. Kuhn, G. R. Paul, A. Malhotra, Y. Kameo, R. Muller, Mechano-Regulation of Trabecular Bone Adaptation Is Controlled by the Local in vivo Environment and Logarithmically Dependent on Loading Frequency. *Front Bioeng Biotechnol* **8**, 566346 (2020).
45. M. L. Bouxsein, S. K. Boyd, B. A. Christiansen, R. E. Guldberg, K. J. Jepsen, R. Müller, Guidelines for Assessment of Bone Microstructure in Rodents Using Micro-Computed Tomography. *Journal of Bone and Mineral Research* **25**, 1468-1486 (2010).
46. F. A. Schulte, F. M. Lambers, G. Kuhn, R. Muller, In vivo micro-computed tomography allows direct three-dimensional quantification of both bone formation and bone resorption parameters using time-lapsed imaging. *Bone* **48**, 433-442 (2011).
47. W. Pistoia, B. van Rietbergen, E. M. Lochmüller, C. A. Lill, F. Eckstein, P. Rüegsegger, Image-based micro-finite-element modeling for improved distal radius strength diagnosis. *J Clin Densitom* **7**, 153-160 (2004).
48. W. Pistoia, B. Van Rietbergen, E. M. Lochmüller, C. A. Lill, F. Eckstein, P. Rüegsegger, Estimation of distal radius failure load with micro-finite element analysis models based on

three-dimensional peripheral quantitative computed tomography images. *Bone* **30**, 842-848 (2002).

49. A. C. Davison, D. V. Hinkley, E. Schechtman, Efficient Bootstrap Simulation. *Biometrika* **73**, 555-566 (1986).

50. R. D. C. Team, in *R Foundation for Statistical Computing*. (Vienna, Austria, 2007).